IN-35

NASA Technical Memorandum 104522

High-Speed Laser Anemometry Based on Spectrally Resolved Rayleigh Scattering

Richard G. Seasholtz
Lewis Research Center
Cleveland, Ohio

Prepared for the
Fourth International Conference on Laser Anemometry
cosponsored by the American Society of Mechanical Engineers, the European Association for Laser Anemometry with Organizational Collaboration and sponsorship from Case Western Reserve University, Cleveland State University, NASA Lewis Research Center, and the Ohio Aerospace Institute
Cleveland, Ohio, August 5–9, 1991

NASA

HIGH–SPEED LASER ANEMOMETRY BASED ON SPECTRALLY RESOLVED RAYLEIGH SCATTERING

R.G. Seasholtz
NASA Lewis Research Center
Cleveland, Ohio 44135

ABSTRACT

Laser anemometry in unseeded flows based on the measurement of the spectrum of Rayleigh scattered laser light is reviewed. The use of molecular scattering avoids the well–known problems (particle lag, biasing effects, seed generation, seed injection) of seeded flows. The fundamental limits on velocity measurement accuracy are determined using maximum likelihood methods. Measurement of the Rayleigh spectrum with scanning Fabry–Perot interferometers is analyzed and accuracy limits are established for both single pass and multi–pass configurations. Multi–pass configurations have much higher selectivity and are needed for measurements where there is a large amount of excess noise caused by stray laser light. It is shown that Rayleigh scattering is particularly useful for supersonic and hypersonic flows. The results of the analysis are compared with measurements obtained with a Rayleigh scattering diagnostic developed for study of the exhaust plume of a small hydrogen–oxygen rocket, where the velocities are in the range 1000 to 5000 m/sec.

INTRODUCTION

Conventional laser anemometry is based on the scattering of light from particles, usually in the size range 0.5 to 2 micrometers diameter. In spite of the general success of this technique, there are severe limitations in certain applications. The introduction of suitable seed material into the flow is often difficult, or simply not feasible, such as in the study of rocket exhausts. Measurements based on single particle measurements are susceptible to a variety of biasing problems caused by correlations between the data rate and the flow parameters. Particle based anemometry also suffers from reduced accuracy when used in highly accelerated, high velocity flows. For these flows, very small seed particles must be used if the particle velocity is to accurately represent the gas velocity. Also, the size of the probe volume must be increased so as not to exceed the frequency response of the photodetectors. The combination of these factors degrades the performance of particle based anemometers in a variety of aerospace research programs. This has led researchers working with high speed flow to examine other approaches to anemometry based on molecular scattering.

Velocity measurement based on the direct interaction of laser light with the gas molecules has several attractive features. Both the need for seeding and any particle lag problems are eliminated. The simplest of the molecular scattering techniques is based on Rayleigh scattering, which is the subject of this paper.

Rayleigh scattering is an elastic process where the internal energy of the molecules is not changed. Thus the frequency of the scattered light is shifted from the frequency of the incident light only by the Doppler effect due to molecular motion. The spectrum of the scattered light contains information about the velocity distribution function of the gas molecules. In particular, the frequency of the peak of the spectrum of the scattered light relative to the frequency of the incident light represents one component of the gas velocity (in the same manner as a conventional reference beam laser anemometer). In this paper, we examine the feasibility of using Rayleigh scattering for velocity measurements in high speed flows. We first look at the fundamental limit on velocity measurement accuracy without consideration of the instrument used to measure the spectrum of the Rayleigh scattered light. We then look at the measurement limits when a Fabry–Perot interferometer is used for measuring the spectrum. In this analysis we include the effects of spurious laser light, which is often a major problem in the application of Rayleigh scattering. We analyze both single pass and multiple pass interferometers. Multiple pass interferometers offer a much higher frequency selectivity and are necessary for situations having a large amount of stray laser light, which is not uncommon for many aerospace test facilities.

An example of nitrogen at ambient temperature and pressure is presented for a range of Mach numbers and spurious light levels. It is shown how the results of this example can be scaled for other flow parameters. We then validate our analysis by applying it to a Rayleigh scattering diagnostic previously developed for use in the exhaust plume of a hydrogen–oxygen rocket, where the velocity is about 5000 m/sec. It is shown that the results of the analysis are consistent with the experimental results.

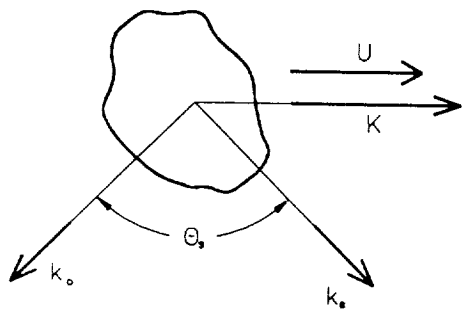

Fig. 1 Scattering diagram for Rayleigh scattering example; scattering angle θ_s=90°

THEORY

Rayleigh scattering

Consider a linearly polarized plane wave with wave vector $\mathbf{k}_o$ (fig. 1) propagating through a gas with a Maxwellian velocity distribution[1]

$$f(\mathbf{v})d^3v = \frac{n}{\pi^{3/2}\,a^3} e^{-c^2/a^2} d^3v \qquad (1)$$

where

$a = (2\kappa T/m)^{\frac{1}{2}}$ = "most probable speed", m/sec
$\mathbf{c} = \mathbf{v}-\mathbf{u}$
κ = Boltzmann's constant (1.38×10^{-23} J/K)
m = molecular mass, kg
n = number density, m^{-3}
T = gas temperature, K
$\mathbf{u}$ = mean velocity, m/sec

The power scattered in the $\mathbf{k}_s$ direction into solid angle $d\Omega$ in frequency interval df is[4]

$$P_s(f)dfd\Omega = I_o\, n\, V_{sc}\left[\frac{d\sigma}{d\Omega}\right]\sin^2\chi\; S(f)\; dfd\Omega \qquad (2)$$

and the mean number of photons in time interval Δt in light frequency interval f_j to $f_j+\Delta f$ is

$$\langle n_j\rangle = \frac{I_o n V_{sc}\lambda\Omega}{hc}\left[\frac{d\sigma}{d\Omega}\right]\sin^2\chi\; S(f_j)\;\Delta f\Delta t \qquad (3)$$

where

$\left[\frac{d\sigma}{d\Omega}\right]$ = Rayleigh differential cross section, m^2/sr
I_o = incident irradiance, W/m^2
V_{sc} = scattering volume, m^3
χ = angle between incident electric field vector and $\mathbf{k}_s$
S(f) = the normalized spectrum of Rayleigh scattered light
Ω = solid angle of light collection optics

For a single component, low density gas (y parameter << 1), the spectrum of the scattered light is[2]

$$S(f)\,df = \frac{2\sqrt{\pi}}{aK} e^{-(2\pi f-\mathbf{K}\cdot\mathbf{u})^2/a^2K^2} df \qquad (4)$$

The width of this Gaussian function is proportional to the square root of the ratio of the gas temperature T to the molecular weight m. The entire spectrum is shifted by a frequency $f_D = \mathbf{K}\cdot\mathbf{u}/2\pi$, where $\mathbf{K}=\mathbf{k}_s-\mathbf{k}_o$ is the wave vector associated with momentum transfer in the scattering, with $\mathbf{k}_s$ and $\mathbf{k}_o$ being the wave vectors of the scattered and incident light. The magnitude of $\mathbf{K}$ is a function of the scattering angle θ_s and the wavelength λ

$$K = |\mathbf{K}| = 2k_o\sin(\theta_s/2) = \frac{4\pi}{\lambda}\sin(\theta_s/2) \qquad (5)$$

We simplify the equation for the spectrum by introducing

$$a' = \frac{aK}{2\pi}, \quad u' = \frac{\mathbf{K}\cdot\mathbf{u}}{2\pi} = \frac{Ku_K}{2\pi} \qquad (6)$$

where u_K is the component of the velocity $\mathbf{u}$ in the $\mathbf{K}$ direction. The spectrum can then be expressed

$$S(f)\,df = \frac{1}{\pi^{1/2}a'} e^{-(f-u')^2/a'^2} df \qquad (7)$$

We also let

$$\Gamma_R = \frac{\epsilon P_o n L_{sc}\lambda\Omega}{hc}\left[\frac{d\sigma}{d\Omega}\right]\sin^2\chi \qquad (8)$$

be the detected photon arrival rate (i.e., photoelectron count rate) of the total Rayleigh scattered light. Here, we used the relation $I_oV_{sc} = P_oL_{sc}$, where P_o is the laser beam power and L_{sc} is the length of the scattering volume along the beam. The overall efficiency factor ϵ accounts for detector quantum efficiency and system losses.

Including spurious light at the laser frequency and broadband noise, the mean number of counts measured in frequency interval f_q to $f_q+\Delta f$ in time interval Δt is

$$\langle n_q\rangle = [\Gamma_R\, S(f_q)\Delta f + \Gamma_w\delta_{ql} + \Gamma_B\Delta f]\Delta t \qquad (9)$$

where Γ_w is the count rate of detected light at the laser frequency (parasitic light scattered from surfaces) and Γ_B is the count rate per unit frequency interval of broadband noise (from dark noise and background light). The Kronecker delta function δ_{ql} = 1 if q=l (where the subscript l refers to the frequency interval containing the laser frequency) and = 0 otherwise.

Cramer-Rao Lower Bound

In general, the spectrum of the scattered light is a function of 5 unknown parameters, which we denote by the vector

$$\boldsymbol{\alpha} = [\Gamma_R,\Gamma_w,\Gamma_B,u_K,T] \qquad (10)$$

The measurement can be described by the vector

$$\mathbf{n} = [n_1, n_2,\ldots,n_q,\ldots] \qquad (11)$$

where the elements of $\mathbf{n}$ are the photoelectron counts for equal frequency intervals Δf in time interval Δt. The Cramer–Rao lower bound for the variance of the estimate of the parameter α_i is[3]

$$V(\hat{\alpha}_i) = [\Gamma^{-1}]_{ii} \qquad (12)$$

where Γ is the Fisher information matrix with elements given by

$$\Gamma_{ij} = -\left\langle \frac{\partial^2 \ln p(\mathbf{n}|\boldsymbol{\alpha})}{\partial\alpha_i\;\partial\alpha_j} \right\rangle \qquad (13)$$

Here, the conditional probability function $p(\mathbf{n}|\boldsymbol{\alpha})$ is the likelihood function, which expresses the probability that given a set of parameters $\boldsymbol{\alpha}$, the set of observations $\mathbf{n}$ will occur. (The

maximum likelihood estimate for the parameters $\boldsymbol{\alpha}$ is given by the $\boldsymbol{\alpha}$ that maximizes $p(\mathbf{n}|\boldsymbol{\alpha})$ for a given set of measurements $\mathbf{n}$.) For Poisson statistics, which we assume apply to the scattered light, the probability of n_q counts in one time interval is

$$p(n_q) = \frac{1}{n_q}\, e^{-\langle n_q \rangle}\, \langle n_q \rangle^{n_q} \tag{14}$$

where the expected value $\langle n_q \rangle$ is given by the equation 9.

The elements of the Fisher information matrix can then be written

$$\Gamma_{ij} = \sum_q \frac{1}{\langle n_q \rangle} \frac{\partial \langle n_q \rangle}{\partial \alpha_i} \frac{\partial \langle n_q \rangle}{\partial \alpha_j} \tag{15}$$

If the parameters are uncorrelated, then the variance of the estimate of each of the parameters is simply the inverse of the corresponding diagonal element of the Fisher matrix, i.e.

$$V_{uc}(\hat{\alpha}_i) = [\Gamma^{-1}]_{ii} = \frac{1}{\Gamma_{ii}} \tag{16}$$

For this case, the lower bound for the variance of the velocity parameter $\hat{u}'$ is

$$V_{uc}(\hat{u}') = \left[\sum_q \frac{1}{\langle n_q \rangle} \left[\frac{\partial \langle n_q \rangle}{\partial u'} \right]^2 \right]^{-1} \tag{17}$$

Using equation 9 for $\langle n_q \rangle$, we obtain

$$V_{uc}(\hat{u}') = \left[\sum_q \frac{1}{[\Gamma_R\, S(f_q) + \Gamma_w \delta_{q1}/\Delta f + \Gamma_B]\Delta f \Delta t} \times \left[\Gamma_R \frac{2(f_q - u')}{a'^2} S(f_q)\, \Delta f \Delta t \right]^2 \right]^{-1} \tag{18}$$

In general, the errors are correlated, and the variance calculated from the inversion of the Fisher matrix (eq. 12) should be used. The simplified expression given by equation 18 should only be used if one is confident that the errors are uncorrelated.

Lower bound for zero background and wall scatter

We can establish simply the lower bound for errors in velocity measurement for the case where spurious light at the laser frequency and background light are negligible. For this case, calculations based on equation 12 show that the velocity error is only weakly correlated with the errors in the other parameters. Thus the simple form for the Cramer–Rao lower bound for the velocity measurement error (eq. 18) can be used, which gives

$$V_{uc}(\hat{u}') = \left[\sum_q \left[\Gamma_R \frac{4(f_q - u')^2}{a'^4} S(f_q)\, \Delta f \Delta t \right] \right]^{-1} \tag{19}$$

We evaluate the sum in equation 19 by allowing $\Delta f \to df$ and converting it to an integral. Performing the integration gives

$$V_{uc}(\hat{u}') = \left[\int_{-\infty}^{+\infty} \Gamma_R \frac{4(f - u')^2}{a'^4} S(f)\, \Delta t\, df \right]^{-1} = \frac{a'^2}{2\Gamma_R \Delta t} \tag{20}$$

Thus the predicted standard deviation in the measurement of the velocity component along K is

$$\sigma(\hat{u}_K) = \frac{a}{(2\Gamma_R \Delta t)^{1/2}} = \left[\frac{2}{\gamma}\right]^{\frac{1}{2}} \frac{c_s}{(2\Gamma_R \Delta t)^{1/2}} \tag{21}$$

where c_s is the speed of sound in the gas and γ is the ratio of specific heats. This shows that, for a fixed Rayleigh scattering count, the error in the velocity measurement is proportional to the speed of sound in the gas. The relative velocity error is

$$\frac{\sigma(\hat{u}_K)}{u_K} = \left[\frac{2}{\gamma}\right]^{\frac{1}{2}} \frac{1}{M_K (2\Gamma_R \Delta t)^{1/2}} \tag{22}$$

where $M_K = u_K/c_s$ can be thought of as the Mach number of the velocity component being measured. Thus the relative accuracy of the velocity measurement improves as the Mach number increases.

RESULTS

Example – Nitrogen at ambient conditions

As an example, consider nitrogen at near–ambient conditions (MW = 28 amu, T = 300 K, p = 14.7 psia = 1.014×10^5 N/m^2, viscosity[4] η = 1.78×10^{-5} N–sec/m^2, Rayleigh differential scattering cross section[5] $(d\sigma/d\Omega)$ = 7.03×10^{-32} m^2/sr). We assume a laser wavelength λ = 514.5 nm, laser power P_o = 1 W, probe volume length L_{sc} = 1 mm, f/4 collection optics (Ω = 0.05 sr), overall efficiency ϵ = 0.01, χ = 90° ("s" scattering), and scattering angle θ_s = 90°. From the ideal gas law, the molecular number density is $n = p/\kappa T = 2.45\times10^{25}$ m^{-3}. Based on these values, the detected count rate from equation 8 is $\Gamma_R = 2.23\times10^6$ counts/sec. The speed of sound $c_s = (\gamma\kappa T/m)^{1/2}$ = 353 m/sec and the most probable molecular speed $a = (2\kappa T/m)^{1/2}$ = 422 m/sec. The scattering wave number $K = (4\pi/\lambda)\sin(\theta_s/2) = 1.727\times10^7$ m^{-1}.

The y parameter[6], which indicates the importance of collective effects, is

$$y = \frac{p}{\eta K a} \simeq 1 \tag{23}$$

Although this value of y puts us in the regime where collective effects start to become important (and the spectrum is no longer strictly Gaussian), we use the Gaussian spectrum for the purposes of our example. The results presented here should generally be valid for gas densities less than 1 amagat (gas density at STP). Note, however, that the deviation from Gaussian would be more important if the spectral shape were being used to determine the gas temperature.

Assuming a data acquisition time of Δt = 1 second, the total number of Rayleigh counts is $G_R = \Gamma_R \Delta t = 2.3\times10^6$, and the Cramer-Rao lower bound (for $\Gamma_w = \Gamma_B = 0$) calculated from equation 21, is

$$\sigma(\hat{u}_K) = 0.2 \text{ m/sec} \tag{24}$$

Thus, for our example, the theoretically lower bound for the velocity error is well within the needs of most experiments. Note that this bound does not depend on the velocity, so the relative error decreases as the velocity increases. This is in marked contrast to particle based anemometry, where the relative error increases as the velocity increases.

Although the theoretical lower bound for velocity measurement is satisfactory, it could only be achieved by using an ideal spectrum analyzer. We know that any real instrument used to measure the spectrum will give less accurate measurements. In the next section we calculate the lower bound for a spectrum measured with a particular instrument – the planar mirror Fabry–Perot interferometer.

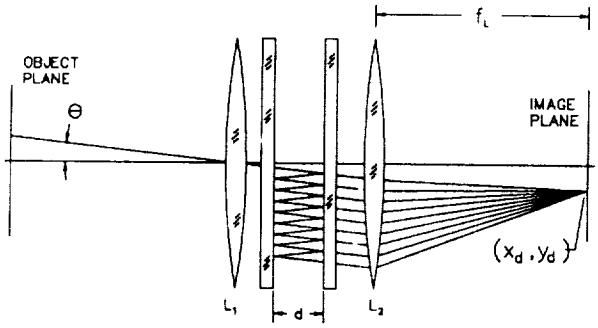

Fig. 2 Fabry–Perot interferometer

Measurement of spectrum using Fabry–Perot interferometer

The Fabry–Perot interferometer[7,8] (fig. 2) is a simple instrument consisting of two parallel, partially transmitting flat mirrors. Its transmittance is a function of the frequency of the incident light, the angle θ of the light with the optical axis, the refractive index μ of the medium between the mirrors, and the mirror separation d. These parameters determine the phase change ψ between successive reflections, which is (neglecting phase change on reflection)

$$\psi = \frac{4\pi\mu d \cos\theta}{\lambda} \tag{25}$$

For a single ray, the transmittance is given by the Airy function

$$I_t = \frac{1}{1 + F \sin^2(\psi/2)} \tag{26}$$

where $F = \sin^{-2}(2N_R/\pi)$, with N_R being the reflective finesse. The Fabry–Perot can function as a scanning spectrum analyzer by measuring the output while varying the mirror spacing d. In practice, the light passed by the interferometer is focused with a lens called the fringe forming lens. An aperture, with radius r, is placed in the focal plane of this lens to define the source area from which light is collected. The usable light collection ability of a planar mirror Fabry–Perot interferometer is given by the étendue U, which is the product of the source area observed and the collection solid angle, i.e.

$$U = \pi r^2 \Omega = \pi r^2 \pi (D/2f_L)^2 \tag{27}$$

where D is the mirror diameter and f_L is the focal length of the collection lens (for simplicity we assume the focal lengths of the collection lens and fringe forming lens are equal). The power that enters the interferometer is then given by the product of the source radiance and the étendue.

The spectrum measured with a Fabry–Perot interferometer can be written[9]

$$\Gamma_m(f_d') = \Gamma_R \int S_R(f') I_R(f_d' - f')\, df' + \Gamma_w I_w(f_d') + B \tag{28}$$

where $f' = f - f_o$ is the frequency shift relative to the laser frequency f_o. The spectrum is a function of the scanning parameter $f_d' = f_o(1 - d/d_o)$, which is related to the mirror spacing d. The mirror spacing d is the physical scanning parameter and varies as a linear function of time from an initial spacing d_o to $d_o + \Delta d$, where Δd is on the order of the wavelength of light. The Rayleigh scattered power Γ_R that enters the interferometer has frequency spectrum $S_R(f')$. The power Γ_w represents the laser light elastically scattered from surfaces. The broadband background light is given by B.

In equation 28, $I_R(f_d')$ and $I_w(f_d')$ are the instrument response functions for Rayleigh scattered light and wall scattered light. The instrument function of the Fabry–Perot is the response to a monochromatic source with the same spatial distribution as the source to be measured[7]. Although $I_R(f_d')$ and $I_w(f_d')$ are not necessarily the same, we assume here, for simplicity, that they are equal (i.e., $I_R(f_d') = I_w(f_d') = I(f_d')$). We also assume that the source has a uniform spatial distribution, so the instrument function can be numerically evaluated using

$$I(f_d') = \frac{1}{A} \int \frac{dA}{1 + F \sin^2\left[\frac{2\pi f_o \mu d_o \cos\theta}{c} \frac{f_o - f_d'}{f_o}\right]} \tag{29}$$

where the integration is over the aperture located in the image plane of the fringe forming lens. The angle θ is the angle of the ray in the interferometer measured from the optical axis. As shown in figure 2, θ can be expressed in terms of the position of the ray at the aperture (x_d, y_d)

$$\theta = \tan^{-1}\left[\frac{\sqrt{x_d^2 + y_d^2}}{f_L}\right] \tag{30}$$

We form the measured spectrum by setting the mirror spacing (and hence the scanning parameter f_d') to fixed number of spacings that we label q, where q=[1,100]. Counts are accumulated for a time Δt at each spacing. The spectrum is then in histogram form with the number of counts in the q^{th} bin given by

$$\langle n_q \rangle = \Gamma_m(f_q)\, \Delta t \tag{31}$$

Fabry–Perot measurements for nitrogen at NTP

In this section we analyze the example discussed above for nitrogen at near–ambient conditions with the scattering geometry shown in figure 1. The predicted error in the measured velocity is the Cramer–Rao lower bound given by equation 12 (equations 15, 31, 29, and 28 are used in the evaluation of equation 12). The integration in equation 29 is done using Gaussian quadrature, and the convolution in equation 28 is done using fast Fourier transforms. The results of this example can be scaled for use with other flows, as is discussed in the following section.

We now consider the measurement of the spectrum using a Fabry–Perot interferometer for the above example (nitrogen at ambient conditions). The Fabry–Perot is used in a scanning mode with the data accumulated in 100 equal time interval bins, so Δt = 0.01 sec with a total data acquisition time of 1 sec. Here, we define $G_R = \Gamma_R \Delta t \times$(number bins) and $G_W = \Gamma_w \Delta t \times$(number bins) as the total number of counts over the entire data acquisition period. (Note that for the previous calculation of the lower bound done without regard to the method of measuring the spectrum, we defined $G_W = \Gamma_w \Delta t$, where Δt was the data acquisition period.) We assume a Fabry–Perot mirror diameter D = 50 mm and a reflective finesse N_R = 20. The Fabry–Perot mirror spacing d and detector aperture size are free parameters and can be selected to minimize the predicted error in the velocity measurement. For a given flow, the uncertainty in the velocity measurement is presented in the form of contour plots as a function of free spectral range and probe volume diameter. Note that the length of the probe volume L_{sc} in equation 8 is determined by the projection of the image of the detector aperture onto the beam (i.e., L_{sc} is a function of both the scattering angle θ_s and the probe volume diameter). We assume that the probe volume diameter is equal to both the diameter of the image of the circular detector aperture and the diameter of the laser beam.

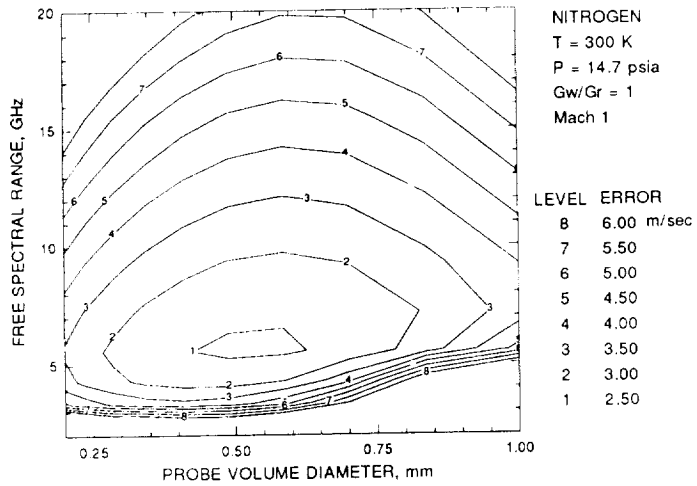

Fig. 3 Predicted velocity measurement error for single pass Fabry–Perot interferometer as a function of probe volume diameter and free spectral range

Each contour plot is based on a 10×10 grid of computed values. The computation time for each contour plot, using a 33 MHz 386 personal computer, was about 700 seconds.

Results were obtained for four Mach numbers (0.2, 1, 2, 4), six values of the ratio of wall scatter to Rayleigh scatter ratio G_w/G_R (0.1, 1, 10, 100, 1000, and 10000), and 1, 3, and 5 pass Fabry–Perot configurations. (The multi–pass transmittance is given by the single pass transmittance, eq. 26, raised to the N^{th} power, where N is the number of passes[10].) Figure 3 shows a representative contour plot for Mach 1, $G_w/G_R = 1$, and single pass. The minimum values of the velocity uncertainty from these contour plots are plotted as a function of G_w/G_R in figure 4. Note that the minima are rather broad in figure 3, so the exact values of mirror spacing and detector size are not critical. (However, the error does increase more rapidly for free spectral range smaller than optimum.) Even for a small amount of wall scatter, the predicted uncertainty in the velocity measurement is about 2 m/sec. This is approximately an order of magnitude larger than the lower bound calculated for measurements obtained with an ideal spectrum analyzer. The primary cause of this difference is that the scanning Fabry–Perot interferometer uses only a fraction of the incident light at any time (that light whose frequency falls with the passband of the interferometer), whereas the ideal spectrum was assumed to use all of the incident light for the entire data acquisition period. As one would expect, as the amount of wall scattered light increases, the accuracy decreases.

Figure 4a is for a single pass Fabry–Perot and shows a large degradation in accuracy for $G_w/G_R \geq 10$. Figures 4b and c show similar data for 3 pass and 5 pass configurations. These show the great improvement in accuracy achievable using multi–pass configurations in experiments with large amounts of wall scattered light. It should be noted that we assumed the same Fabry–Perot mirror diameter for these multi–pass configurations as was used for single pass. Although this could be achieved, in principle, by operating interferometers in series, the usual technique is to use a single interferometer with retroreflectors to obtain multiple passes[10]. This method greatly reduces the effective mirror aperture, which decreases the amount of usable Rayleigh scattered light. In addition, the losses in the Fabry–Perot increase with the number of passes. For example, a single pass interferometer with 75% peak transmission would only have 42% and 24% transmission when operated in 3 pass and 5 pass configurations, respectively. Finally, for sake of comparison, the predicted velocity

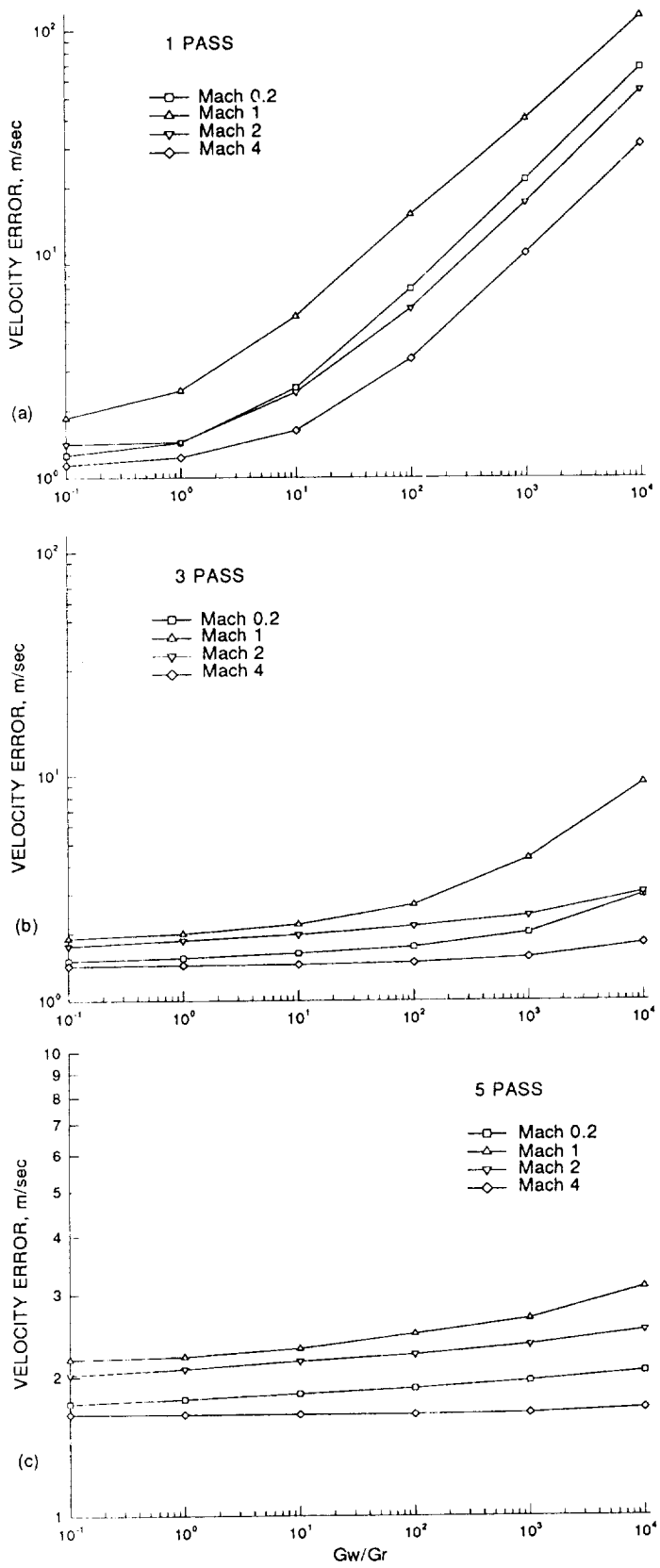

Fig. 4 Predicted minimum velocity measurement error as function of ratio of wall scatter light to Rayleigh scatter light for nitrogen at 300 K: (a) single pass Fabry–Perot (b) 3 pass (c) 5 pass

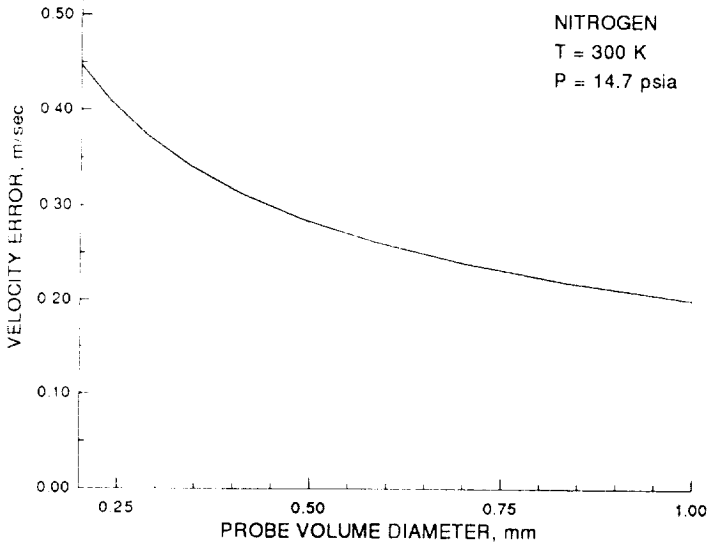

Fig. 5 Predicted uncertainty in velocity measurement for ideal spectrum analyzer

measurement error for an ideal spectrum analyzer is shown in figure 5 (with the error plotted as a function of probe volume diameter). Note that an ideal spectrum analyzer would not be affected by wall scatter light that is located in an infinitely narrow bandwidth.

Scaling of results

In general, the predicted error in the velocity measurement is proportional to the speed of sound in the gas and inversely proportional to the square root of the number of detected photons. This is the relation found for the case of the theoretical lower bound (eq. 21), and was verified for calculations made for the Fabry–Perot with large amounts of wall scatter and for multi–pass configurations. This relation permits the results obtained for the above example to be extended to other situations. We consider two examples.

The first example of scaling is a low density (0.01 amagat), Mach 4, nitrogen flow having a static temperature of 900 K. Compared to the ambient condition example, the Rayleigh counts would be decreased by a factor of 100, and the ratio G_w/G_R would increase by the same factor (assuming the same amount wall scatter), say from 1 to 100, and the sonic velocity would increase by a factor of $3^{1/2}$ due to the higher temperature. For a single pass Fabry–Perot, using figure 4a, we see that the velocity error would be $(3.3)(10)3^{1/2} = 57$ m/sec, or about 2.4%.

The second example of scaling is a Mach 1, nitrogen flow at ambient temperature and pressure in an experiment with a large amount of wall scatter, such as one would typically have in an internal flow. Because of the assumption of a large amount of wall scatter, we select a 5 pass Fabry–Perot. We assume that the effective mirror diameter is 7 mm, and the losses in the Fabry–Perot are such that the efficiency is only 0.25% instead of the 1% in the above example. These differences cause the Rayleigh count rate to be reduced by a factor of about 200, which corresponds to an increase of the predicted error in the velocity by a factor of 14. Using this factor with figure 4c, the predicted error is about $(3)(14) = 42$ m/sec, or 12%. Here, we might consider extending the data acquisition time (e.g., increasing the time from 1 second to 10 seconds would decrease the predicted error to 13 m/sec, or 4%).

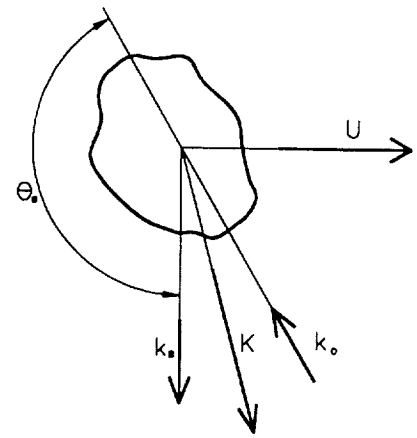

Fig. 6 Scattering diagram for hydrogen–oxygen rocket measurements; scattering angle θ_s=152.8°

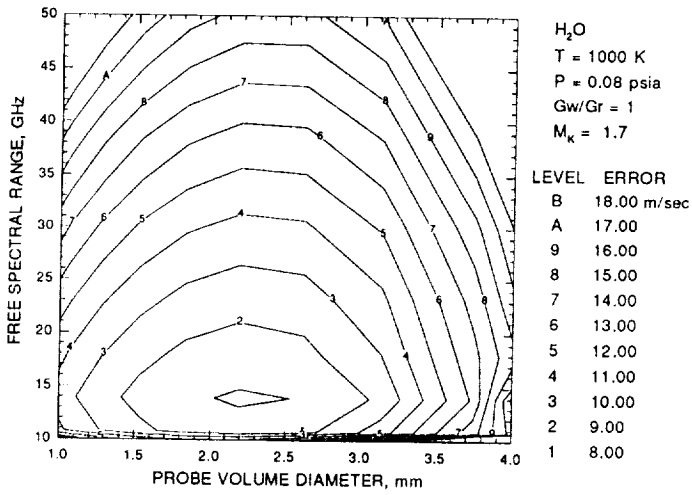

Fig. 7. Predicted velocity measurement error for hydrogen–oxygen rocket exhaust measurements

Comparison with experimental results from H_2–O_2 rocket

We now apply our prediction analysis to a Rayleigh scattering diagnostic developed for a small (100 N thrust) hydrogen–oxygen rocket test facility. This system and the experimental results obtained with it are described in reference 11. The relevant parameters for the H_2O exhaust gas are: MW=18, γ=1.25, p=0.08 psia, T=1000 K, V=5000 m/sec, θ_s=152.8°, $(d\sigma/d\Omega)=5.01\times10^{-32}$ m²/sr. The single pass Fabry–Perot used had an entrance aperture of 64 mm and a mirror spacing of 7.0 mm (FSR = 21.4 GHz). A 1 W argon–ion laser was used at λ = 514.5 nm. The light was linearly polarized perpendicular to the scattering plane, so χ=90°. As shown in the scattering diagram (fig. 6), the measured velocity component was about 75° from the actual velocity, so the Mach number of the measured component of the flow was M_K = 1.7. The probe volume diameter was 2.2 mm and length was 4 mm. Spectral data were collected for 90 seconds. Assuming an overall efficiency of 1%, the expected detected Rayleigh scattering count rate (from eq. 8) is Γ_R = 3300 counts/sec. For measurements taken on the centerline of the exhaust plume, the measured Rayleigh count rate was about 5000 counts/sec. The background count rate was about 250 counts/sec, and the ratio G_w/G_R typically was about 1.

Applying our analysis to this flow and Fabry–Perot configuration gives the predicted error shown in figure 7. From

this figure, the optimum probe volume diameter is 2.6 mm (close to the value of 2.2 mm used in the experiment). From figure 7, we see that the optimum free spectral range is 14 GHz, which is somewhat less than the experiment value of 21.4 GHz However, this would only reduce the error by about 20%. The predicted Rayleigh count rate is about 4800 counts/sec, which is close to the value obtained in the actual measurements. This indicates that our assumption of 1% overall efficiency is reasonable.

CONCLUDING REMARKS

The prediction analysis applied to the measurement of velocity based on the spectral measurement of Rayleigh scattered light with a planar mirror Fabry–Perot interferometer indicates its feasibility for a variety of flow conditions. In experiments where the amount of wall scattered light cannot be reduced to low levels, the use of a multi–pass Fabry–Perot offers a means to achieve adequate frequency selectivity.

The use of a scanning Fabry–Perot interferometer precludes instantaneous velocity measurements. Even with relatively high Rayleigh scattering levels, several seconds per measurement point will probably be required. In rotating systems, the measurements would need to be correlated with the angular position of the rotating part, thus further increasing the data acquisition time.

The material presented here considered only the measurement of a single velocity component. The method, however, can be extended to multiple components in a straightforward manner by adding either additional receiving optics, or by adding additional input beams.

It is important to note that the velocity measurements described in this paper are not sensitive to the exact molecular composition of the gas (because the mean velocity of the gas is determined by the frequency of the spectral peak of the Rayleigh scattered light). Furthermore, if a large, uniform concentration of small particles is present in the flow, the velocity measurement can be made using the light scattered from the particles. (Examples of particle scattered light used to measure velocity using a confocal Fabry–Perot are presented in references 12 and 13). If a small number of relatively large particles are in the flow, they will scatter large amounts of light compared to the molecular Rayleigh scattering, and the spectral data can be screened to eliminate the anomalously large values caused by the particles.

Finally, we would like to emphasize that: (1) since the predicted relative error decreases with Mach number, the Rayleigh scattering technique is particularly suited to supersonic and hypersonic flow studies; and (2) because the velocity measured is the actual molecular velocity, highly accelerated flows, including flows with shocks, can be accurately mapped.

REFERENCES

1. J.O. Hirschfelder, C.F. Curtiss, and R.B. Bird, "Molecular Theory of Gases and Liquids", John Wiley & Sons, 1954, p. 101.

2. I.L. Fabelinskii, "Molecular scattering of light", Plenum Press, 1968, p. 263.

3. A.D. Whalen, "Detection of signals in noise", Academic Press, 1971, pp. 324–331.

4. R.C. Reid, J.M. Praussnitz, and B.E. Poling, "The properties of gases and liquids" , 4th Ed., McGraw–Hill, 1987, p. 399.

5. W.C. Gardiner, Jr., Y. Hidaka, and T. Tanazwa, "Refractivity of combustion gases", Comb. and Flame 40, 1981, pp. 213–219.

6. R.P. Sandoval and R.L. Armstrong, "Rayleigh–Brillouin spectra in molecular nitrogen", Phys. Rev. **A13**, 1976, pp. 752–757.

7. J.M. Vaughan, "The Fabry–Perot Interferometer, History, Theory, Practice and Applications", Adam Hilger, Bristol, 1989, Chapter 3.

8. G. Hernandez, "Fabry–Perot Interferometers", Cambridge University Press, Cambridge, 1986, Chapter 3.

9. P.A. Wilksch, "Instrument Function of the Fabry–Perot Interferometer", Applied Optics 24, 1985, pp. 1502–1511.

10. Sandercock, "Some recent developments in Brillouin scattering", RCA Rev. **36**, 1975, pp.89–107.

11. R.G. Seasholtz, F.J. Zupanc, and S.J. Schneider, "Spectrally Resolved Rayleigh Scattering Diagnostic for Hydrogen–Oxygen Rocket Plume Studies", AIAA 29th Aerospace Sciences Meeting", Reno, AIAA paper 91–0462, 1991.

12. R.G. Seasholtz and L.J. Goldman, "Three component velocity measurements using Fabry–Perot interferometer", Second International Symposium on Applications of Laser Anemometry to Fluid Mechanics, Lisbon, 1984.

13. R.G. Seasholtz and L.J. Goldman, "Combined fringe and Fabry–Perot laser anemometer for three component velocity measurements in turbine stator cascade facility", AGARD CP–399, (also NASA TM–87322), 1986.

NASA
National Aeronautics and Space Administration

Report Documentation Page

1. Report No.	2. Government Accession No.	3. Recipient's Catalog No.
NASA TM-104522		

4. Title and Subtitle
High-Speed Laser Anemometry Based on Spectrally Resolved Rayleigh Scattering

5. Report Date

6. Performing Organization Code

7. Author(s)
Richard G. Seasholtz

8. Performing Organization Report No.
E-6395

10. Work Unit No.
505-62-50

9. Performing Organization Name and Address
National Aeronautics and Space Administration
Lewis Research Center
Cleveland, Ohio 44135-3191

11. Contract or Grant No.

13. Type of Report and Period Covered
Technical Memorandum

12. Sponsoring Agency Name and Address
National Aeronautics and Space Administration
Washington, D.C. 20546-0001

14. Sponsoring Agency Code

15. Supplementary Notes
Prepared for the Fourth International Conference on Laser Anemometry cosponsored by the American Society of Mechanical Engineers, the European Association for Laser Anemometry with organizational collaboration and sponsorship from Case Western Reserve University, Cleveland State University, NASA Lewis Research Center, and the Ohio Aerospace Institute, Cleveland, Ohio, August 5-9, 1991. Responsible person, Richard G. Seasholtz, (216) 433-3754.

16. Abstract
Laser anemometry in unseeded flows based on the measurement of the spectrum of Rayleigh scattered laser light is reviewed. The use of molecular scattering avoids the well-known problems (particle lag, biasing effects, seed generation, seed injection) of seeded flows. The fundamental limits on velocity measurement accuracy are determined using maximum likelihood methods. Measurement of the Rayleigh spectrum with scanning Fabry-Perot interferometers is analyzed and accuracy limits are established for both single pass and multi-pass configurations. Multi-pass configurations have much higher selectivity and are needed for measurements where there is a large amount of excess noise caused by stray laser light. It is shown that Rayleigh scattering is particularly useful for supersonic and hypersonic flows. The results of the analysis are compared with measurements obtained with a Rayleigh scattering diagnostic developed for study of the exhaust plume of a small hydrogen-oxygen rocket, where the velocities are in the range 1000 to 5000 m/sec.

17. Key Words (Suggested by Author(s))	18. Distribution Statement
Laser anemometers Rayleigh scattering Fabry-perot interferometers	Unclassified - Unlimited Subject Category 35

19. Security Classif. (of the report)	20. Security Classif. (of this page)	21. No. of pages	22. Price*
Unclassified	Unclassified	8	A02

NASA FORM 1626 OCT 86

*For sale by the National Technical Information Service, Springfield, Virginia 22161

NASA